

Eccentricity Evolution in Simulated Galaxy Clusters

Stephen N. Floor^{1,4}, Adrian L. Melott¹, Christopher J. Miller², and Greg L. Bryan³

ABSTRACT

Strong cluster eccentricity evolution for $z \leq 0.13$ has appeared in a variety of observational data sets. We examine the evolution of eccentricity in simulated galaxy clusters using a variety of simulation methodologies, amplitude normalizations, and background cosmologies. We do not find such evolution for $z < 0.1$ in any of our simulation ensembles. We suggest a systematic error in the form of a redshift-dependent selection effect in cluster catalogs or missing physics in cluster simulations important enough to modify the cluster morphology.

Subject headings: cosmology: galaxy clusters: evolution –large-scale structure of universe

1. Introduction

Galaxy clusters are the largest bound objects in the Universe. They provide information on gravitational instability, and understanding their formation is helpful in describing the transition to nonlinearity in structure formation.

In studies of a variety of optical and X-ray samples, Melott, Chambers, and Miller (2001, hereafter MCM) and Plionis (2002) found significant evolution in the gross morphology of galaxy clusters over the redshift range 0 to 0.13. When projected galaxy clusters were fit to ellipses by a variety of procedures, their eccentricities were found to evolve on a timescale comparable to one or two crossing times for the clusters. The inclusion of X-ray data is important, as it is much less subject to projection effects than optical data. In all cases, with varying significance, the clusters were found to have become less eccentric at lower z . It was argued that this could be understood as a relaxation process in a low-density

¹Department of Physics & Astronomy, University of Kansas, Lawrence, KS 66045

²Department of Physics & Astronomy, Carnegie Mellon University, Pittsburgh, PA 15213

³Department of Astrophysics, Oxford University, Oxford, UK OX1 3RH

⁴snfloor@ku.edu

cosmological background, made possible by a greatly reduced recent merger rate. Mergers tend to occur by infall along supercluster filaments (Shandarin and Klypin 1984; Colberg et al. 1999) which can lead to alignment of the cluster axis (Binggelli 1982; Chambers, Melott, & Miller 2002, and references therein) as well as aligned bulk flows within the cluster (Novikov et al. 1999).

This poses new questions of structure formation for cosmological simulations. Will cluster eccentricity evolution appear there? Does it depend on the initial conditions, the background cosmology, and/or the physics included within given simulations?

Richstone, Loeb, & Turner (1992) showed that cluster morphology could be used as a diagnostic of mass density in the Universe. While a cosmological constant, λ , was argued to have little effect, a large mass density Ω_m would produce more irregular clusters due to recent formation; on this basis they argued $\Omega_m \geq 0.5$. Mohr et al. (1995) looked at a variety of simulations, finding their $\Omega_m = 1$ simulations closest to the distribution of axial ratios for observed clusters, since low- Ω_m simulations produced too-spherical clusters. Jing et al. (1995) disagreed, noting that open or λ -dominated flat cosmologies also produced substantial irregularity in clusters. Using the terminology OCDM and λ CDM for these, and τ CDM for the $\Omega_m = 1$ case (with the same initial conditions), they found increasing irregularity and eccentricity in the order OCDM, λ CDM, τ CDM. They found the effect of λ was smaller for increasing Ω_m , as one would expect. They did not explore evolution. Thomas et al. (1998) reinforced these conclusions. Suwa et al. (2003) presented results on ellipticity evolution, comparing clusters only at $z = 0$ with those at $z = 0.5$ (but not intermediate redshifts). These results suggest that OCDM clusters are slightly rounder than λ CDM, although again the difference is small and not significant in their study. They found a small amount of ellipticity evolution between the two redshifts.

We are interested in exploring the evolution of eccentricity in the recent past, especially for redshifts $0 \leq z \leq 0.1$, where there is a variety evidence for evolution in the data. For this reason we have emphasized the outer regions of clusters, and used methods similar to those applied to many observed clusters.

2. Simulations

We examined projected cluster properties in a variety of simulations based on Cold Dark Matter and Gaussian perturbations (hereafter CDM). One set has been previously described and extensively used elsewhere (Loken et al. 2002, and references therein). We refer to this as the λ CDMH simulation, to distinguish its inclusion of hydrodynamics from

other, purely N-body simulations we studied. This simulation focused on the most massive objects within a region $256 h^{-1} Mpc$ on a side in a flat, cosmological-constant dominated universe ($\Omega_0 = 0.3$, $\Omega_\lambda = 0.7$) with a baryon fraction of $\Omega_b = 0.026$ and a Hubble constant of 70 km/s/Mpc. The initial conditions used the Eisenstein & Hu (1999) parameterization of the CDM power spectrum, normalized to an amplitude corresponding to $\sigma_8=0.93$, where σ_8 is the rms density fluctuation inside spheres of radius $8 h^{-1} Mpc$. The dark matter particle mass was $1.3 \times 10^{10} M_\odot$ and the evolution of the gas was followed with an Adaptive Mesh Refinement method (see Bryan 1999) that solves the equations of hydrodynamics (not including radiative cooling, thermal conduction, or star formation) on a grid. The method starts off with a relatively coarse mesh but decreases the mesh spacing in dense region so that the smallest cell size (best resolution) achieved was $16 h^{-1} kpc$. We used X-ray images assuming a metallicity of 0.3 of solar in the 0.5-2.0 keV bandpass. We used previously saved data on 11 clusters taken at $z = 0.25$, 0.1, and 0, identified using the ‘‘HOP’’ algorithm (Eisenstein and Hut 1998, hereafter EH). This algorithm finds regions above some threshold density, and merges them, associating them with regions of some maximal density δ_{peak} . These regions are merged into a single region (‘‘cluster’’, for our purposes) if they lie within a contour of density δ_{saddle} . Any associated particles are also considered part of the cluster if they lie within a connected contour above the density δ_{outer} . The parameters used to identify these clusters were 480, 400, and 160 for δ_{peak} , δ_{saddle} , and δ_{outer} , respectively. For more details on this method see EH. In the λ CDMH, the mesh-refinement method requires following the same volume element, chosen by the presence of a cluster at $z = 0$, through its evolution. Clusters at higher redshift are taken from this volume; it is possible that in this case they may not be the most massive clusters in the large simulation volume at earlier times. Another substantial difference with the larger cluster sample which will be analyzed next is that these very massive clusters correspond to a Richness in excess of 2. In fact they are even more massive than typical $R = 2$ clusters, but less than $R = 3$ clusters. It is not possible to change this given the AMR method, although checking the conclusions against other (N-body) simulations constitutes a partial cross-check.

We conducted another, larger, ensemble of pure Nbody simulations. All used the same initial power spectrum, corresponding to CDM (Bardeen et al. 1986) with $\Gamma=\Omega h=0.225$. This was evolved in both an open ($\Omega_{m0}=0.34$, OCDM1), a flat matter-dominated ($\Omega_{m0}=1$, τ CDM), and a flat cosmological-constant model ($\Omega_{m0}=0.34$, $\Omega_{\lambda0}=0.66$, λ CDM1) Inclusion of the τ CDM model was motivated by the wish to see whether major differences in the expansion rate affected the eccentricity. All three of these ensembles were run as before, to an amplitude corresponding to $\sigma_8=0.93$. A Hubble Constant $h = 2/3$ was used in the simulation analysis. These N-body runs had three realizations each of 256^3 particles in boxes of $128 Mpc$ diameter. Given the volume and target space density of $R \geq 1$ clusters, 6

clumps were extracted from each of these three simulation "boxes". For consistency with our previous observational analyses, we simulated clusters of Richness $R \geq 1$. Volume-limited samples exist for such clusters, but not for Richness 0. We used parameters 400, 200, 80 for HOP in this case, in analogy with densities of observed clusters and virialization density thresholds. Having identified clumps with HOP, clusters were identified with the N most massive clumps in the simulation corresponding to a mean separation of $50h^{-1}$ Mpc. We therefore have a total of 18 clusters from our three realizations. Given two independent axial ratios out of three projections, we have 54 views at each redshift which have the statistical weight of 36 views. In other words, this simulation ensemble produces the equivalent of 36 independent observed clusters for each assumed background cosmology. (We have the equivalent weight of 22 views in the λ CDMH runs.) The dark matter particle mass was $5.2 \times 10^9 M_\odot$ in the low Ω_m model and proportionally larger in the high Ω_m model. Data was taken at moments corresponding to $z=0.2, 0.1$ and 0 in the OCDM1 and τ CDM simulations.

In the OCDM1 boxes, our selected objects ranged from about 8×10^{13} to $1 \times 10^{15} M_\odot$, for the mass within an Abell radius. This agreement with the mass range of observed clusters is a consistency check on our procedure. In the τ CDM box, they were about three times more massive, as expected for consistency with the assumed background cosmology. In the λ CDMH box, the range was from about 5×10^{14} to $2 \times 10^{15} M_\odot$, appropriate for $R > 2$ clusters.

Having chosen these clusters, three Cartesian projections were constructed. There are only two independent axial ratios, a/b , and b/c , therefore only two independent ratios in projection, whether we project along cluster principal axes or not. We project along the simulation coordinate axes, since we do not want to prefer principal axes; we use all 3 axes for balance. In order to take account of this partial lack of independence, we recognize that the standard deviation of our results is smaller by a factor of $\sqrt{\frac{2}{3}}$ than if they were fully independent. This is taken into account in all statistical results quoted here.

After initial analysis of OCDM1, we decided to examine more closely the possible effect of amplitude normalization. We therefore reran the entire ensemble with lower values of $\sigma_8=0.78$ and 0.58, called OCDM2 and OCDM3 respectively. Naturally, these clusters are somewhat less massive than in OCDM1. Likewise, λ CDM2 has $\sigma_8=0.83$.

We have 33 projections of λ CDMH simulations at each redshift, and 54 of each of the OCDM*, λ CDM*, and τ CDM simulations. Including the fact that each of these is viewed at three redshift stages, our simulated cluster sample size is larger than any of the individual data samples studied in MCM, though not as large as the APM sample used by Plionis (2002).

Fair sampling is a consideration here. We are viewing the same overall simulation volume, and in most cases, the same clusters, at a variety of redshifts. This is obviously not true in the observed samples. If this were important, cosmological simulations as currently analyzed would be of limited relevance to understanding structure formation. Separate simulations would be needed for each redshift bin. We partially compensate for this effect (which we assume to be small) in the OCDM^* , λCDM^* , τCDM simulations by identifying clusters separately in each redshift bin. This occasionally resulted in the selection of different objects at different stages of evolution.

In the λCDMH , the mesh-refinement method requires following the same volume element, chosen by the presence of a cluster at $z = 0$, through its evolution. Only the most massive clusters in this simulation were chosen for mesh refinement. The space density and threshold mass for the objects chosen corresponds to a richness $R > 2$. Clusters at higher redshift are taken from this sub-volume; it is possible that in this case they may not be the most massive clusters at that z in the large simulation volume. An additional caveat in the application of the λCDMH group is therefore its correspondence to richer clusters. However, according to the study of Plionis (2002), ellipticity evolution is not weaker for richer clusters.

3. Determination of Eccentricity

Observers had widely varying procedures for selecting which portions of clusters to analyze, and in some cases the procedure was not specified. When major and minor projected axes were found, varying definitions of ϵ , the ellipticity, were applied. In fact, varying definitions of ellipticity appear in common use in mathematics, physics and astronomy literature. We followed one well-specified procedure and a standard definition of *eccentricity*, fitting ellipses to our projected clusters. This geometrical term is well-known, and not subject to the ambiguity in definitions of “ellipticity”. For an ellipse with major and minor axes a and b respectively, the eccentricity e is defined by

$$e = \sqrt{1 - \frac{b^2}{a^2}} \quad (1)$$

this definition of e is also used for ϵ by some, but not all, work which reports on “ellipticity”. Another common definition of ellipticity, $\epsilon = 1 - b/a$, has e and ϵ increasing monotonically with one another inside their useful ranges from 0 to 1. Our statistical inferences, discussed later, are nonparametric and based on ranks; thus they would be the same whether we used e or ϵ .

Only projected information is available for observed clusters in useful precision, so we study our simulated clusters in projection. The center of these objects was defined for most

analyses here as the center of mass of the linked particles. It must be stated clearly that the procedures used in observational studies are not uniform, or even always clearly specified. This center of mass is our closest possible analog for the center of mass of the optically luminous matter—the galaxies. In the case of the λ CDMH simulation set, we also analyzed the synthetic X-ray emission of the clusters. In this case, we chose as a center the region of strongest simulated surface brightness in the X-ray. For the sake of fuller exploration, we repeated this procedure using the highest peak of the projected mass density as the center, and found no qualitatively different conclusions after referring our computation to the center of mass of regions drawn from around this center.

We selected the widely used “annulus method”; it emphasizes the outer regions of the cluster, which is important in trying to measure ellipticity for highly centrally concentrated X-ray images. This is the most widely used method in cluster ellipticity work. For each cluster projection, having chosen a center as described above, a circle of radius $1.5 h^{-1}Mpc$ was drawn about this point. Then another circle of smaller radius was placed so that the annulus between them had 0.2 times the entire mass enclosed within the outer circle. The purpose of using annuli is to emphasize outer regions, especially important for highly concentrated, emission-weighted X-ray images. We repeated this procedure using $2.0 h^{-1}Mpc$, with no qualitatively different conclusions. We also examined the eccentricity of our clusters when the entire mass within $1.5 h^{-1}Mpc$ was used rather than an annulus. Although eccentricity values were generally lower, our conclusions again were qualitatively the same. We further tested the robustness of our conclusions against procedure by dropping the annulus procedure, and computing the values based on the entire region connected by the HOP procedure. This also shifted the values somewhat, but did not change our conclusions about evolution. The results quoted herein are based on the $1.5 h^{-1}Mpc$ annulus.

We computed the “inertia tensor” \mathbf{I} of this annulus with respect to its center of mass (center of emission for X-ray images). Very few observational studies mentioned that they used the center of mass frame; we hope that they did since the results are nearly meaningless without. If not computed with respect to the center of mass, the eigenvalues have no particular relationship to the axes of the object. We used the conventional definition

$$I_{ij} = \sum m_{\alpha}(\delta_{ij}r^2 - x_{\alpha i}x_{\alpha j}) \quad (2)$$

where we sum over regions α .

The eigenvalues of \mathbf{I} are proportional to a^2 and b^2 , as defined above, for a homogeneous ellipse. In this way we define the eccentricity of the projected simulated cluster approximated as an ellipse.

4. Results

In Table 1 below, we show for the λ CDMH simulation, the median and mean e at each redshift bin, as well as the standard deviation of the mean. Note that the standard deviation in the estimate of the mean is smaller than the standard deviation of one measurement. Figures 1 and 2 contain histograms of the eccentricity for the OCDM1, τ CDM, and λ CDMH ensembles. Note that in λ CDMH, we show eccentricity inferred both from the dark matter distribution, which is a stand-in for the optical studies, assuming that galaxies reasonably trace the dark matter; we also show results derived from the inferred X-ray luminosity. There are weak evolutionary trends, but none as steep as that seen in the data. Again, note that this data sample corresponds to very rich clusters.

In agreement with previous studies, we find weakly increasing eccentricity in the order OCDM1, λ CDM1, τ CDM at $z = 0$.

We also performed a Wilcoxon rank-sum test (Lehman 1998) to compare samples at different stages of evolution and with one another. A nice feature of this test is that it will give the same results for comparing measures which are nonlinearly related, but monotonically increasing functions of one another, like e and ϵ . In this case, the null hypothesis is that the lower- z sample does not have systematically smaller eccentricity than the high- z sample. In the last column, we give the confidence in rejection of eccentricity evolution (reduction with lower z). In particular, the number in this column is the probability that the change in eccentricity seen in the simulations could result from random draws of a cluster population which did not have decreasing eccentricity. The first number given in the last column is the confidence resulting from comparison with the cluster ensemble on that line with the ensemble on the following line (next higher redshift datafile). The following number (in parentheses) is the confidence resulting from comparison with the ensemble two redshift bins higher (i.e. between redshift 0 and 0.2 or 0.25) Small values of P_W correspond to the direction of evolution seen in the data.

Although there is a significant signal in a variety of both optical and X-ray data samples that galaxy clusters have undergone a morphological evolution, becoming significantly more circular since $z = 0.1$, we have not found this in our ensemble of simulations. There is such evolution only in the OCDM1 and λ CDM1 simulation sample for $0.1 \leq z \leq 0.2$. OCDM3 has evolution in the opposite sense over the same redshift interval. Evolution found in data by MCM was found only for $z \leq 0.1$; that found by Plionis was for $z \leq 0.18$ and in fact appeared concentrated in lower redshift ranges. It was confirmed (Plionis, personal communication) that no significant ellipticity evolution appears in that sample for $z \geq 0.13$. Despite the differences in codes and lesser differences in cluster selection procedures, none of the simulated samples showed strong eccentricity evolution over the crucial period $0 \leq$

$z \leq 0.1$. Evolution similar to that found in most of the data would correspond roughly to eccentricity dropping from about 0.8 to 0.7 during that period, which would stand out with high significance in our simulations.

There is a slightly different situation with the APM cluster sample. The evolution rate is slower there; it would correspond to mean eccentricity changing from about 0.76 to 0.70 during the redshift interval 0.1 to 0. (extrapolating its slope). This is a dangerous extrapolation, since this sample does not contain information for $z < 0.038$, and its rate of evolution appears to steepen for lower z . Such a steepening would be consistent with the more rapid rate of evolution found at lower redshifts in all but one of the MCM samples.

It should be mentioned that the APM cluster sample was selected in a somewhat different way than the controlled Abell/ACO sample used elsewhere. These clusters were initially found by selecting regions of a high overdensity in a smaller region, about half the diameter typically used in the Abell catalog (Dalton et al. 1997). This procedure might produce a selection effect accounting for the difference.

To summarize, the APM sample would appear to be consistent with the rate of evolution in many of our samples at about the 2σ level, if extrapolated linearly to $z=0$.

5. Discussion

In some way, the simulations as we have analyzed them do not faithfully model the observed “local” Universe. There are a variety of ways to account for this; we will mention a few.

We initially used a normalization $\sigma_8=0.93$. There is a hint in the OCDM1 results that a lower normalization might produce the strong evolution seen in the data in the redshift range needed. We decided to test this, and the OCDM2 and OCDM3 results provide evidence against this hypothesis (see Table 1 and Figure 3). We also wished to investigate cosmic variance beyond the simple variation of random phases in the initial conditions. Density fluctuations on the scale of the N-body box should be no more than about 10% *rms*. As an aggressive test of cosmic variance, we reran OCDM1 in a background with $\Omega_{m0}=0.2$. This also would be an effective test of any possible effects due to our being located in a very large underdense region, such as that suggested by Buswell et al. (2003) and Frith et al. (2003). We found no significant change in the results of the ensemble.

The most obvious possibility is observational selection effects. The sign of the effect needed is that more eccentric clusters are included in cluster surveys when they are far away

than when they are close.

The data used in MCM and Plionis (2002) are based on optical cluster catalogs. In MCM, they used subsets of the Abell/ACO catalogs that had published ellipticities (in either X-ray or optical). Plionis (2002) used a subset of the Automated Plate Machine (APM) clusters as published in Dalton et al. (1997), with ellipticities as given in Basilikos, Plionis, and Maddox (2000). Plionis (2002) also looked at Abell/ACO clusters in their APM sample and found the same ellipticity evolution as for the entire sample.

In the optical and Xray samples examined in MCM, ellipticity appears to increase with redshift for all samples. This increase exists in all samples studied in both papers, but the way in which it appears is different for different samples: (1) a lack of nearby highly elliptical clusters (compared to higher redshift); (2) an increase in the number of highly elliptical clusters at higher redshift (compared to nearby); (3) a lack of highly circular clusters at high- z (compared to low- z); and of course any combination of these. In fact, there are observed samples consistent with all of these possibilities (MCM, Plionis 2002). It is worthwhile asking whether selection effects (both at the low- z and the high- z end of the cluster samples) could play a role in this correlation.

For instance, it is possible that both the APM and the Abell/ACO catalogs are incomplete at low redshifts and that those clusters missing from the sample have significant ellipticity. Likewise, an incompleteness in circular clusters at higher redshifts is also possible. This latter case seems less plausible, since such “regularly” shaped clusters should be easy to identify. Ebeling et al. (1999) claimed that high levels of substructure will lead to a decreased probability of cluster selection. The selection function for regularly shaped (circular) clusters should be stable over the range of redshifts examined in MCM and Plionis et al. In this case it is doubtful that circular clusters would be preferentially missed at higher redshifts.

However, Adami et al. (2000) conducted extensive testing on their X-ray cluster selection function (for the Serendipitous High-Redshift Cluster (SHARC) survey (Romer et al. 2000)). They reported that highly elliptical clusters were *more easily* found at high redshift. Adami et al. note that for a fixed cosmology, an elliptical cluster will have a higher central surface brightness than a circular cluster with the same luminosity. They found that this effect was only significant at the high- z limit of the SHARC survey, where the selection function is very sensitive to the central surface brightness of a cluster. All redshifts simulated by Adami et al. were greater than the ones considered here. In spite of this objection, it is possible that elliptical clusters could be more easily detected at high- z and that some highly circular clusters could be missed at high- z . Since all of the samples examined in MCM and Plionis et al. were optically selected, one would have to assume that an analogous effect

could be present in optical samples.

In general, it remains unclear how ellipticity affects the selection of clusters. The argument made by Ebeling et al. (1999) that clusters with substructure are harder to detect, need not necessarily translate into elliptical clusters being harder to detect. The use of extensive simulations (as in Adami et al. 2000) is probably a requirement before any conclusions can be drawn regarding a ellipticity evolution in any given dataset. Unfortunately, the selection procedures used for the cluster samples in Plionis (2002) and MCM are so complicated that their selection functions are too difficult to model. Our best hope is to examine the next generation of cluster catalogs (e.g. from the Sloan Digital Sky Survey) whose completeness and selections should be well-measured.

It is possible that the method of defining included mass and computing eccentricity could affect these results. However, we also explored using a *friends of friends* algorithm, as well as various HOP parameters, and abandoning the annulus method in favor of inclusion of all mass in the clusters. None of these changed the evolution of eccentricity, though some changed its amplitude (consistently over redshifts, so as to preserve the lack of evolution).

Another possibility is that the simulations are missing crucial physics which might induce this change. Although violent relaxation may isotropize objects through the time-dependent gravitational potential, we cannot exclude processes in the hot gas which is the dominant baryonic component of the clusters. Radiative cooling may cause the gas to contract, gravitationally entraining some of the dark matter. Also, it has been shown (Narayan and Medvedev 2001) that thermal conduction may be important, especially in the turbulence following major mergers.

6. Acknowledgments

We thank M. Plionis and G. Evrard for useful comments. SNF and ALM gratefully acknowledge the support of the National Science Foundation through grant AST-0070702, especially a supplement for Research Experiences for Undergraduates. Invaluable computing support came from the National Center for Supercomputing Applications.

REFERENCES

Adami, C., Ulmer, M. P., Romer, A. K., Nichol, R. C., Holden, B. P., & Pildis, R. A. 2000, ApJS, 131, 391

- Bardeen, J.M., Bond, J.R., Kaiser, N., & Szalay, A.S. 1986, ApJ304, 15
- Basilakos, S., Plionis, M., & Maddox, S. 2000, MNRAS, 316, 779
- Binggeli, B. 1982, A&A 107, 338
- Bryan, G.L. 1999, Computing in Science and Engineering, 1:2, 46
- Busswell, G.S., Shanks, T., Outram, W.J., Firth, N., Metcalfe, N., & Fong, R. 2003, astro-ph/0302330
- Chambers, W.C., Melott, A.L., & Miller, C.J. 2002, ApJ, 565, 849
- Colberg, J.M., White, S.D.M., Jenkins, A., & Pearce, F.R. 1999, MNRAS, 308, 593
- Chambers, S.W., Melott, A.L., & Miller, C.J. 2002, ApJ, 565, 849
- Dalton, G. B., Maddox, S. J., Sutherland, W. J., & Efstathiou, G. 1997, MNRAS, 289, 263
- Ebeling, H. et al. 2000, ApJ, 534, 133
- Eisenstein, D.J., & Hut, P. 1998, ApJ, 498, 137
- Eisenstein, D.J., & Hu, W. 1999, ApJ, 518, 2
- Firth, W.J., Busswell, G.S., Fong, R., Metcalfe, N., & Shanks, T. 2003, astro-ph/0302331
- Jing, Y.P., Mo, H.J., Börner, G., & Fang, L.Z. 1995, MNRAS, 276, 417
- Lehman, E.L. 1998, Nonparametrics (Upper Saddle River: Prentice-Hall)
- Loken, C. et al. 2002 ApJ 579, 571
- Melott, A.L., Chambers, S.W., & Miller, C.J. 2001, ApJ, 559, L75
- Mohr, J.J., Evrard, A.E., Fabricant, D.G., & Geller, M.J. 1995, ApJ, 447, 8
- Narayan, R., & Medvedev, M.V. 2001 ApJ Letters, 562, L129
- Novikov, D.I., Melott, A.L., Wilhite, B.C., Kaufman, M., Burns, J.O., Miller, C.J., and Batuski, D.J. 1999, MNRAS, 304, L5.
- Plionis, M. 2002, ApJ, 572, L67.
- Richstone, D., Loeb, A., & Turner, E.L. 1992 ApJ 393, 477
- Shandarin, S.F., and Klypin, A.A., 1984, Sov Astron. 28, 491

Suwa, T., Habe, A., Yoshikawa, K., & Okamoto, T. 2003 ApJ, 588, in press (astro-ph/0108308)

Thomas, P.A., et al., 1998, MNRAS, 296, 1061

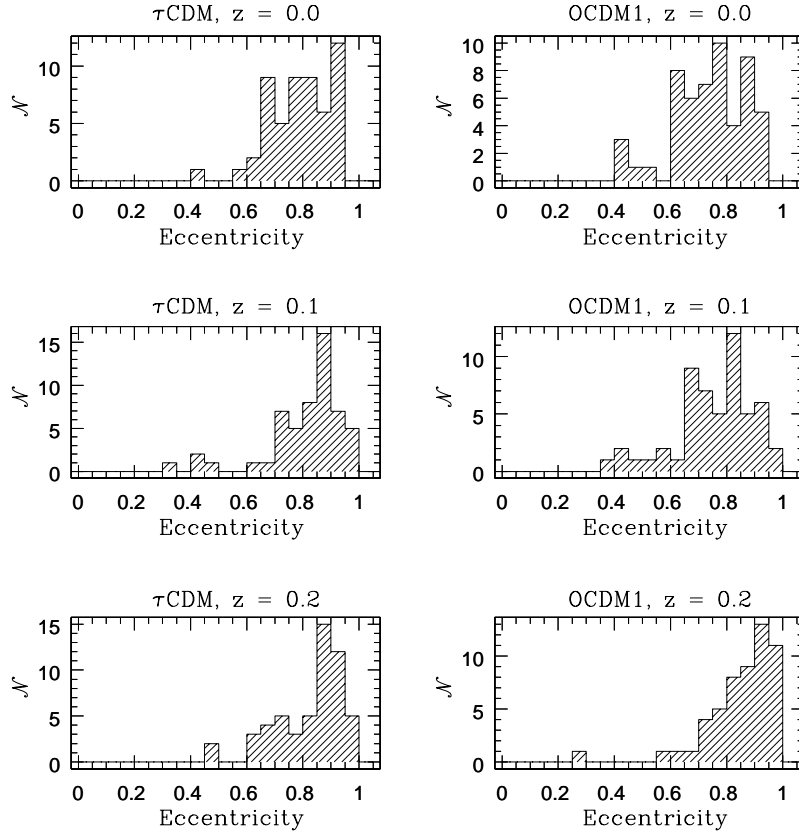


Fig. 1.— Distribution of eccentricity for the OCDM1 (low Ω) and τ CDM (high Ω) clusters at redshifts 0, 0.1, and 0.2.

Table 1. λ CDMH Cluster Eccentricities, $N=33$, $R > 2$

Simulation type	σ_8	Redshift	Median e	Mean e	$\sigma_e(\text{mean})$	P_W
λ CDMH (mass)	0.93	0.	.63	.61	.027	.24 (.16)
λ CDMH (mass)	–	0.1	.66	.63	.028	.46
λ CDMH (mass)	–	0.25	.68	.64	.026	–
λ CDMH (X-ray)	0.93	0.	.61	.66	.036	.33 (.34)
λ CDMH (X-ray)	–	0.1	.73	.68	.033	.65
λ CDMH (X-ray)	–	0.25	.70	.67	.029	–

Table 2. N-body Cluster Eccentricities, $N=54$, $R \geq 1$

Simulation type	σ_8	Redshift	Median e	Mean e	$\sigma_e(\text{mean})$	P_W
OCDM1	0.93	0.	.75	.74	.018	.27 (5×10^{-5})
OCDM1	–	0.1	.77	.76	.019	4×10^{-4}
OCDM1	–	0.2	.89	.85	.016	–
λ CDM1	0.93	0.	.77	.78	.014	.045 (7×10^{-4})
λ CDM1	–	0.1	.83	.80	.020	.033
λ CDM1	–	0.2	.88	.85	.015	–
τ CDM	0.93	0.	.80	.79	.014	.12 (.036)
τ CDM	–	0.1	.86	.81	.018	.19
τ CDM	–	0.2	.87	.83	.016	–
OCDM2	0.78	0.	.87	.83	.017	.21 (.076)
OCDM2	–	0.1	.88	.85	.015	.57
OCDM2	–	0.2	.89	.86	.015	–
OCDM3	0.58	0.	.89	.84	.018	.11 (.98)
OCDM3	–	0.1	.90	.85	.017	.99
OCDM3	–	0.2	.83	.77	.023	–
λ CDM2	0.83	0.	.85	.83	.015	.030 (.017)
λ CDM2	–	0.1	.88	.86	.014	.47
λ CDM2	–	0.2	.89	.86	.016	–

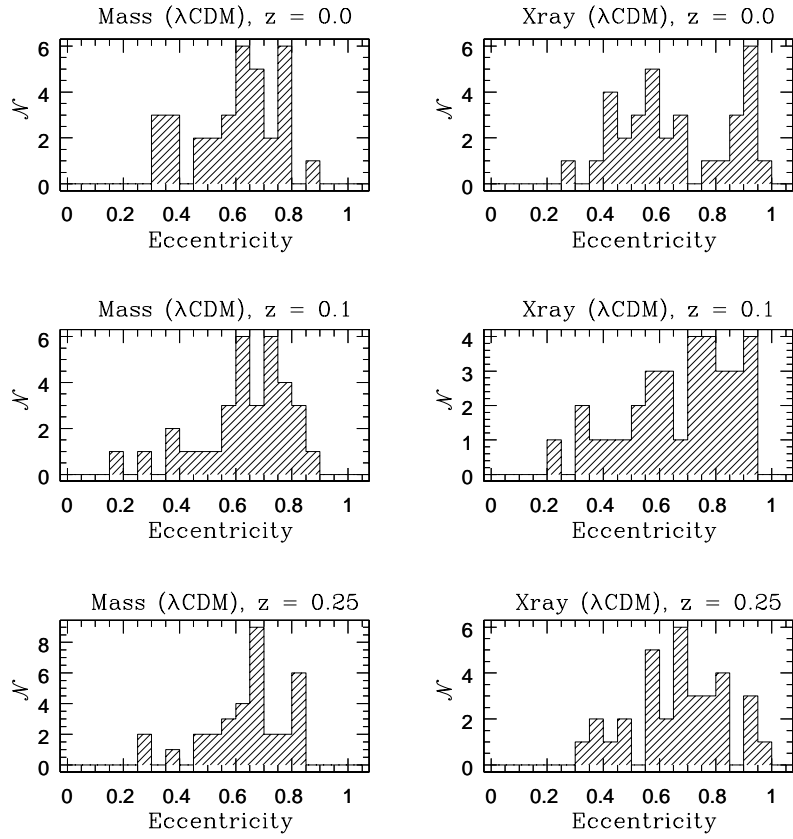


Fig. 2.— Distribution of eccentricity for the λ CDMH clusters at redshifts 0, 0.1, and 0.25. The eccentricity of the mass distribution and of the simulated X-ray emission are plotted separately.

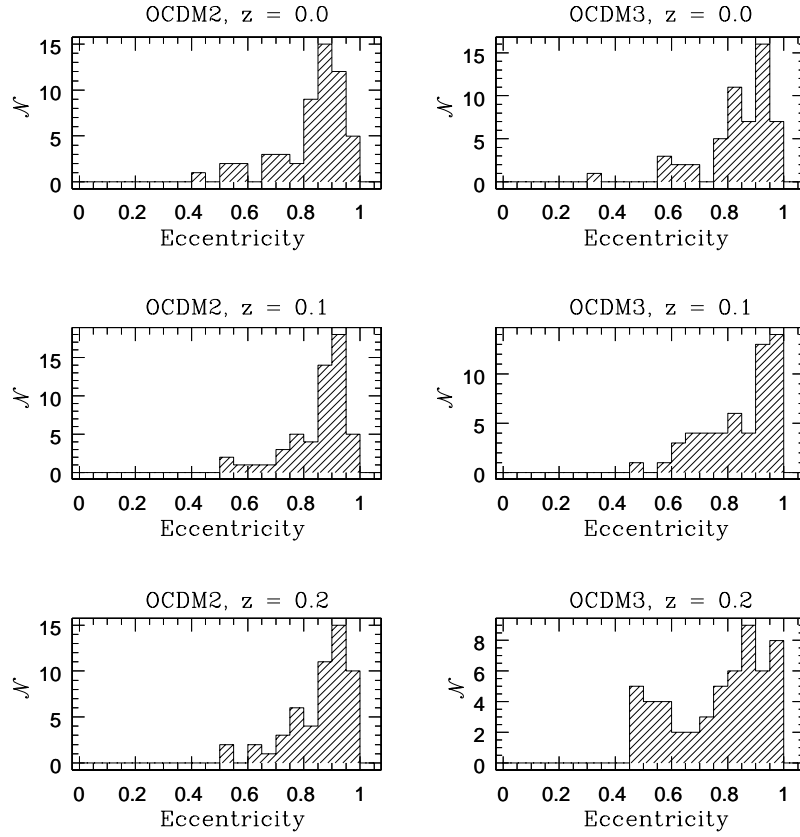


Fig. 3.— Distribution of eccentricity for the OCDM2 and OCDM3 (low Ω_m , low normalization: see text) clusters at redshifts 0, 0.1, and 0.2.